SCIENTIFIC REPORTS

OPEN

SUBJECT AREAS:
APPLIED PHYSICS
NANOPARTICLES
RENEWABLE ENERGY
NANOSCALE MATERIALS

Received
31 July 2012

Accepted
25 September 2012

Published
13 November 2012

Correspondence and requests for materials should be addressed to M.M.H. (muhammadmustafa.hussain@kaust.edu.sa)

Nano-materials Enabled Thermoelectricity from Window Glasses

Salman B. Inayat, Kelly R. Rader & Muhammad M. Hussain

Integrated Nanotechnology Lab, Electrical Engineering, Physical Science and Engineering King Abdullah University of Science and Technology, Thuwal 23955-6900, Saudi Arabia.

With a projection of nearly doubling up the world population by 2050, we need wide variety of renewable and clean energy sources to meet the increased energy demand. Solar energy is considered as the leading promising alternate energy source with the pertinent challenge of off sunshine period and uneven worldwide distribution of usable sun light. Although thermoelectricity is considered as a reasonable renewable energy from wasted heat, its mass scale usage is yet to be developed. Here we show, large scale integration of nano-manufactured pellets of thermoelectric nano-materials, embedded into window glasses to generate thermoelectricity using the temperature difference between hot outside and cool inside. For the first time, this work offers an opportunity to potentially generate 304 watts of usable power from 9 m^2 window at a 20°C temperature gradient. If a natural temperature gradient exists, this can serve as a sustainable energy source for green building technology.

Thermoelectricity is considered as one of most interesting alternate clean energy sources. Its application ranges from large-scale power generation using wasted heat from industrial processes, vehicle exhaust, and spacecraft[1]. It is quiet in operation, highly reliable and typically can harvest energy as long as a reasonable temperature gradient exists. Thermoelectricity is generated when two dissimilar temperature regions are joined by a pair of thermocouples made up of suitable thermoelectric materials. Thermoelectric materials hence convert the thermal gradient into thermoelectricity. Several factors influence the physics: thermoelectric properties (Seebeck coefficient, thermal conductivity and electrical conductivity) and temperature difference between the hot and cold zones. The figure of merit for a thermoelectric material is generally expressed by:

$$ZT = \left(\sigma S^2/k\right) T$$

Where ZT is the figure of merit, S is the Seebeck coefficient, $ó$ is electrical conductivity, k is thermal conductivity and T is temperature difference. Since 1950s, researchers have focused on increasing the ZT above 1. Thermal conductivity k is comprised of a lattice component k_L and an electronic component k_e. With this intriguing relationship, any attempt to increase the electrical conductivity, therefore, results in thermal conductivity increment too. Therefore, the progress in thermoelectric materials from the perspective of making a game changer transformation is still limited.

At the same time, evolution of nanotechnology has opened up new frontiers such as low dimensional quantum dots and super-lattices and mechanical alloying of thermoelectric materials. They have resulted in lower thermal conductivity while retaining the electrical conductivity and Seebeck coefficient. Venkatasubramanian et. al. have achieved the highest reported ZT of 2.4 in p type Bi_2Te_3/Sb_2Te_3 super lattices at 300K[2] by growing phonon blocking electron transmitting hetero-structures by low temperature metal organic chemical vapor deposition (MOCVD) technique. Harman et. al. used molecular beam epitaxy (MBE) to grow PbSeTe/PbTe quantum dot super-lattices with ZT of 1.6 at 300K[3]. Poudel et. al. used BiSbTe nano-crystalline bulk materials made by hot pressing nano-powders ball milled from crystalline ingots to reduce the thermal conductivity due to phonon scattering at the grain boundaries resulting in a ZT of 1.4 at 373K[4]. Most of these methods use either expensive process technologies such as MOCVD and MBE or use energy intensive processes.

While the search for improved ZT is continuing, we have explored a novel idea to leverage the existing thermoelectric materials and nano-manufacturing techniques to generate thermoelectricity from naturally existing temperature difference between solar heated outside and relatively cool inside of buildings especially in the geographic locations which experience lengthy summer or reasonably higher temperature like 30°C or above. Nearly 50% of the world population experiences such average temperature. In addition to thermoelectric

generation during the hot day time, our thermoelectric nano-materials embedded window glasses can generate appreciable thermoelectricity even during off sunshine hours to serve as supplemental clean energy source.

The major challenge with such approach is the window glass (or the "*in between*" interface) itself. In the past, reported thermoelectric generators using micro-fabrication techniques include either a lateral or a vertical design but they are fabricated on one side of the interface[5–9]. With conventional vertical designs, several μm thick thermocouples are possible. Although with lateral designs longer thermocouples are possible however their placement through a solid interface such as window glass is not practical. Therefore, we have hot pressed nano-materials ball milled from commercially purchased thermoelectric materials to make thermoelectric pellets. Next, we made holes inside 5 mm thick glass and inserted those pellets periodically. Finally we used copper based interconnects to connect them to complete the thermoelectric generators. Our initial experimental result with only 4 pellets shows 0.112 μW of power at a temperature gradient of 23.5°C with bismuth telluride ($Bi_{1.75}Te_{3.25}$) and antimony telluride (Sb_2Te_3) alloyed with sulfur as n and p-type materials, respectively. This work projects nearly 304 watts of seamless power generation from 9 m^2 window at a 20°C temperature difference if the best reported thermoelectric materials are used[4,10].

For our demonstration we have chosen commercially available $Bi_{1.75}Te_{3.25}$ and Sb_2Te_3 (Beijing Cerametek Materials Inc.). At first, we prepared two sets (ball milled) by loading Sb_2Te_3 and $Bi_{1.75}Te_{3.25}$ in separate planetary ball mill jars with ball to powder ratio of 15:1 and were subjected to 24 hours of ball milling at 300 rpm. The next two sets (sulfur added) were alloyed with 6% sulfur and then were ball milled same as the first two sets. We made stainless steel molds with 5 mm inner diameter to match the exact diameter of the holes drilled in window glasses. The 5 mm mold design eliminates the unnecessary delay involved in cutting smaller pellets out of a large tablet pressed using conventional large sized dies. The mold also resulted in vertical pillar like pellets pressed to the thickness that is equal to thickness of the window glass. Next we retrieved the vertical pellets 5 mm to 7 mm long. All six different samples (ball milled nano-materials, sulfur added ball milled nano-materials and as purchased thermoelectric powders) were prepared by pressing at 320°C at 100 MPa for 1 hour using Carver bench top heated press – a less energy intensive tool.

We used inductively coupled plasma – optical emission spectroscopy (ICP-OES), x-ray diffraction (XRD), scanning electron microscope (SEM), and transmission electron microscope (TEM) to study the physical characteristics of the thermoelectric materials.

Results

ICP - OES results of all the six samples verified the elemental composition and ratios of each element present in the samples. Minor variations observed in the compositions of the main elements (Bi, Sb and Te) are due to the effect of ball milling. In order to validate the fidelity of the ICP - OES, all the samples were cross examined with x-ray flourescence (XRF). The XRF results closely matched with that of the ICP - OES. We believe the thermoelectric properties of the ball milled samples can be further modulated by increasing the sulfur content[10]. XRD pattern for all six samples show that ball milling decreased the size of the as-purchased powders (Fig. 1a, b). SEM pictures of the six samples confirm the XRD results (Fig. 2a, b, c, d, e, f). The TEM samples preparation required polishing followed by ion milling. The TEM images confirm uniform crystallinity and particle size agreeing well with the XRD results (Fig. 3a, b).

We characterized the thermoelectric properties of the samples independently before integration into the window glasses. The Quantum Design™ Physical Properties Measurement System (PPMS) was used for these measurements. We mounted 5 mm long pellets on the sample puck for thermal transport measurements. We used two-probe techniques to obtain the Seebeck coefficient and thermal conductivity of the samples. We measured the electrical conductivity of the pellets using four-probe AC resistivity option in PPMS by soldering copper wires to the top face of the pellets.

Electrical resistivity of as-purchased, ball milled and sulfur added samples of $Bi_{1.75}Te_{3.25}$ shows that the electrical resistivity of the as-purchased sample is the highest while it is lower for the ball milled and sulfur added samples due to higher carrier concentration (Fig. 4a). Electrical resistivity of as-purchased, ball milled and sulfur added samples of Sb_2Te_3 shows a similar trend as that of the $Bi_{1.75}Te_{3.25}$ with as-purchased samples having the highest resistivity values compared to the ball milled and sulfur added samples due to lower carrier concentration (Fig. 4b). Seebeck coefficient of as-purchased, ball milled and sulfur added samples of $Bi_{1.75}Te_{3.25}$ shows that the as-purchased sample has the highest Seebeck coefficient as

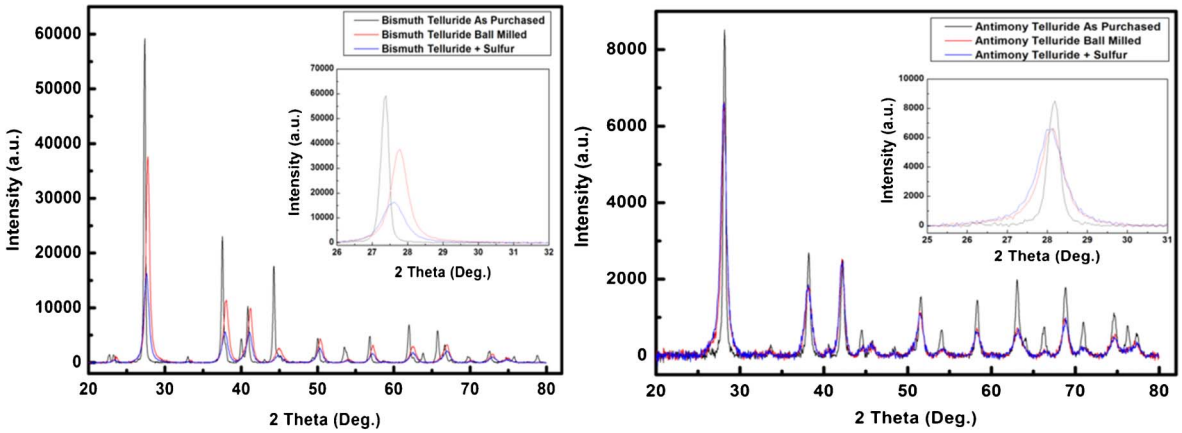

Figure 1 | X-ray diffraction analysis of as purchase, ball milled and ball milled sulfur alloyed $Bi_{1.75}Te_{3.25}$ and Sb_2Te_3. In case of $Bi_{1.75}Te_{3.25}$, the peaks for all three samples have different intensities and widths with the as-purchased sample having the tallest and narrowest peak verifying that this sample has the largest particle size (a). The peaks for ball milled and sulfur added samples are also shifted relative to each other. The peak for sulfur added sample shows the smallest particle size which indicates that the individual sulfur powder that was added and ball milling does not reduce the particle size of $Bi_{1.75}Te_{3.25}$ powder to a value comparable to the size of individual sulfur powder particles. In case of Sb_2Te_3, the peak widths for ball milled and sulfur added samples are broadened relative to the peak for as-purchased sample verifying the size reduction with ball milling (b). Moreover the widths for ball milled and sulfur added samples closely overlap suggesting that ball milling reduced the particle size of Sb_2Te_3 powders to a value equal to the size of individual sulfur powder particles. The inset is the close up of the major peaks centered near 27 degrees for $Bi_{1.75}Te_{3.25}$ and around 28 degrees for Sb_2Te_3.

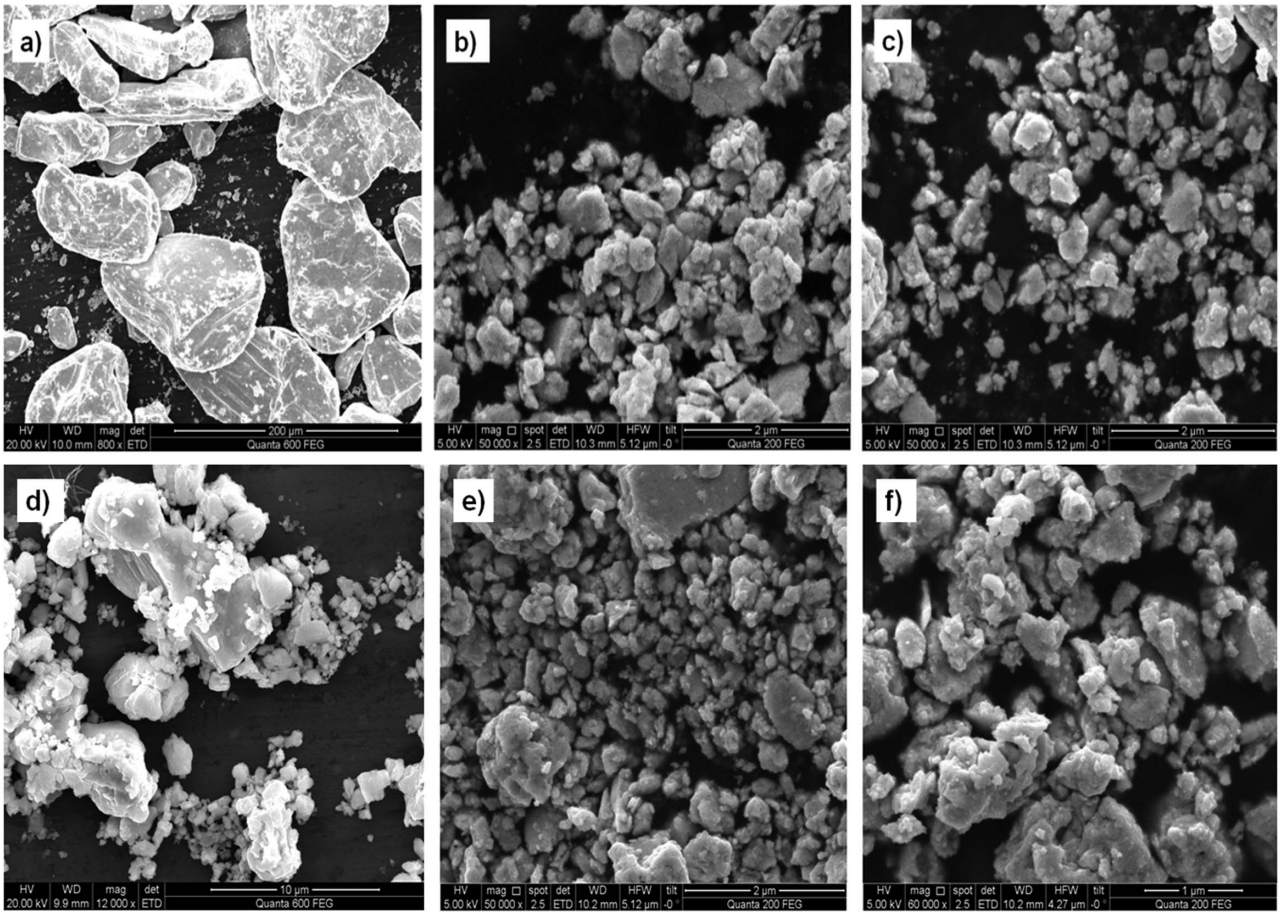

Figure 2 | Scanning electron microscopic images of as purchase, ball milled and ball milled sulfur alloyed $Bi_{1.75}Te_{3.25}$ and Sb_2Te_3. In general the ball milled nano-materials are much smaller than the as-purchased micro-sized samples: $Bi_{1.75}Te_{3.25}$ and Sb_2Te_3, respectively (a and d). The average particle size of ball milled $Bi_{1.75}Te_{3.25}$ is slightly larger than the sulfur added samples (b and c). On the other hand, ball milled samples of Sb_2Te_3 without sulfur have comparable particle size to the samples with sulfur added (e and f).

expected for having the lowest electrical conductivity and carrier concentration (Fig. 4c). During thermal conductivity measurement, we observed significant decrease in the thermal conductivity for the ball milled and sulfur added nano-materials samples of $Bi_{1.75}Te_{3.25}$ and Sb_2Te_3.

To measure power generation, we placed the proto-type window glass with 4 thermoelectric pellets made up of $Bi_{1.75}Te_{3.25}$ and Sb_2Te_3 alloyed with sulfur between a glass slide and a heat sink and then placed on a hot plate (Fig. 5 inset). We applied thermal paste between each interface as an attempt to ensure all pellets were subjected to

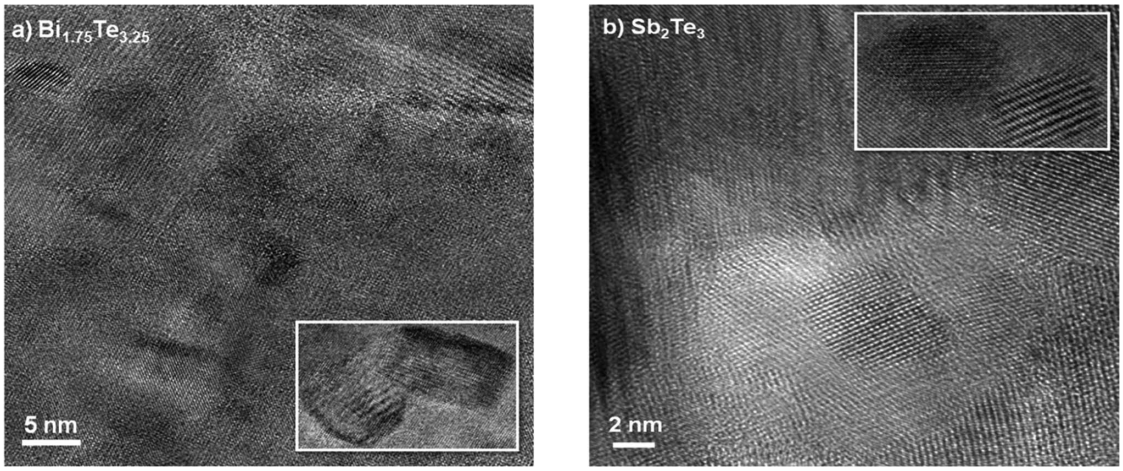

Figure 3 | Transmission electron microscopic images of ball milled $Bi_{1.75}Te_{3.25}$ and Sb_2Te_3. TEM image showing the microstructure of pellet hot pressed from ball milled $Bi_{1.75}Te_{3.25}$ sample (a). Inset shows sharp angular boundaries. Closer examination of the TEM results also shows the presence of smaller particles embedded inside the grains. These smaller particles may have been produced during hot pressing or may have been the results of non uniform ball milling. TEM image showing the microstructure of pellet hot pressed from ball milled Sb_2Te_3 sample (b). Inset shows close packing of grains.

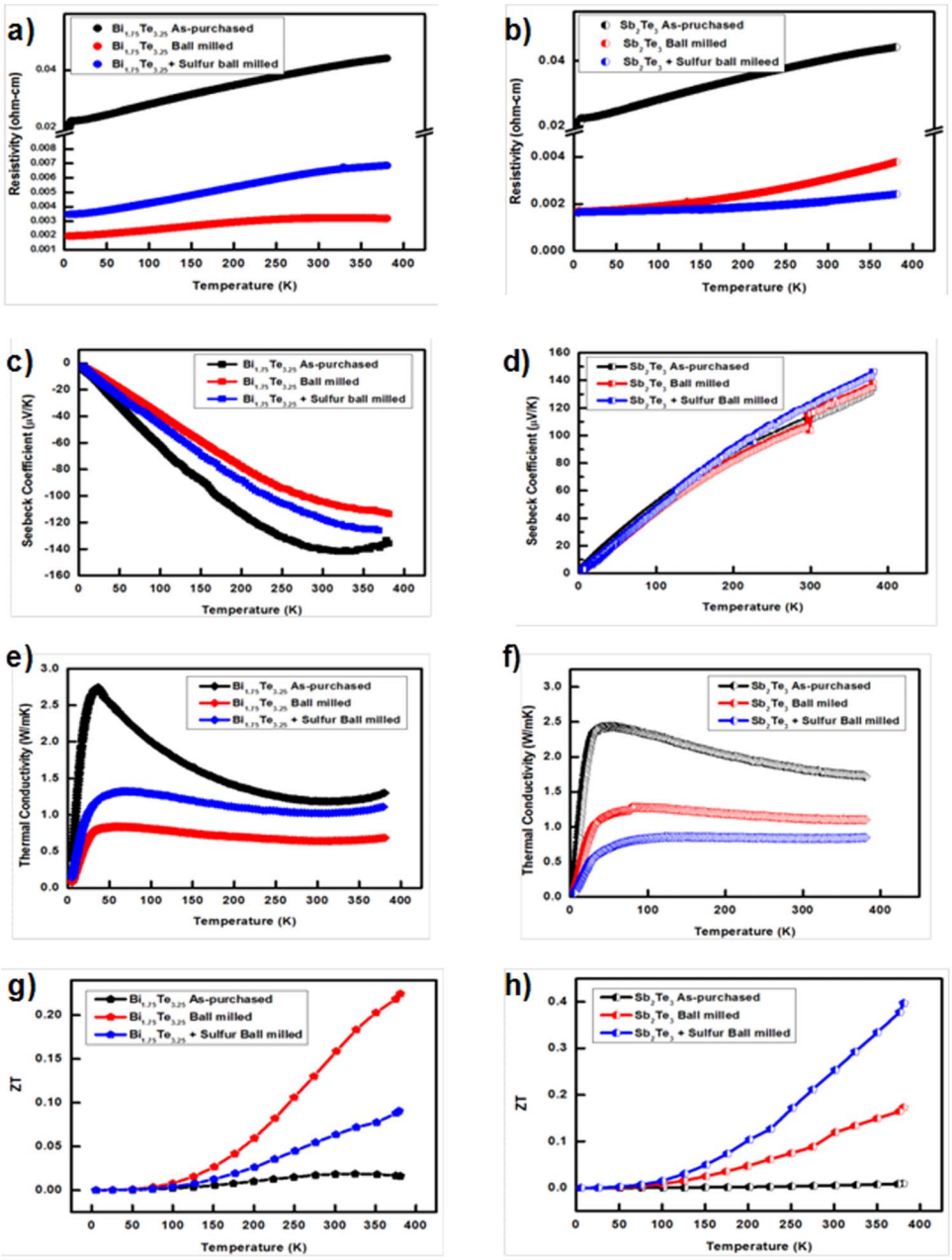

Figure 4 | Electrical and thermoelectric properties of as purchased, ball milled and ball milled sulfur alloyed $Bi_{1.75}Te_{3.25}$ and Sb_2Te_3. Detail explanations of the characteristics are given in the main article.

uniform heat flux. We carried out the electrical testing for various temperature gradients. We ramped up the hot plate temperature in uniform intervals with ample thermal delay to allow the opposite surface of the glass slide to attain a stable hot side temperature. The hot side temperature, T_h, and cold side temperature, T_c, were measured using thermocouples placed on each side of the device. We found the measured output power for a temperature gradient of 23.5°C is 0.112 μW.

Discussion

SEM pictures of the six samples show that the ball milled samples of Sb_2Te_3 without sulfur have comparable particle size to the samples with sulfur added, whereas the average particle size of ball milled $Bi_{1.75}Te_{3.25}$ is slightly larger than the sulfur added samples. The TEM images show a slight increase in grain sizes with hot pressing can be seen from the TEM pictures. In case of $Bi_{1.75}Te_{3.25}$ the grains have sharp angular boundaries that can be responsible for boundary scattering of phonons resulting in lower thermal conductivity. The smaller entities observed in ball milled $Bi_{1.75}Te_{3.25}$ pellets compared to pellets formed from the as-purchased powders are believed to cause further rattling of phonons inside the system, lowering the thermal conductivity to smaller values with overall enhancement of figure of merit. TEM images of pressed pellet of Sb_2Te_3 show fine grains that they are closely packed with circular shapes without any presence of smaller embedded particles. The circular boundaries are believed to have caused lesser scattering of phonons compared to the phonon scattering occurring in $Bi_{1.75}Te_{3.25}$ samples with angular grain boundaries. The effect of circular grains and the absence of embedded particles are evident from relatively smaller reduction in thermal conductivity in pellets pressed from ball milled powders of Sb_2Te_3 than the as-purchased counterpart compared to the difference seen

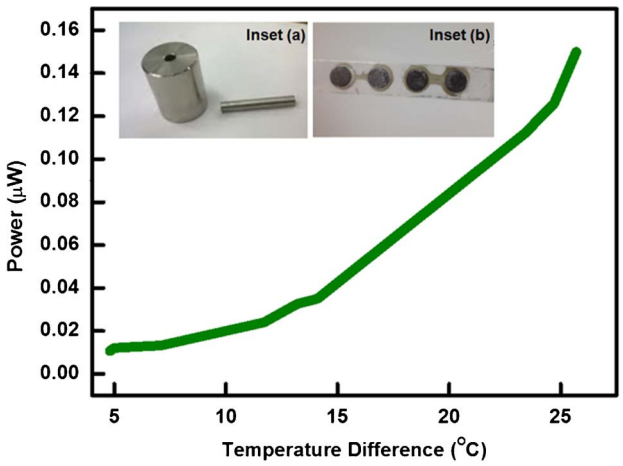

Figure 5 | Thermoelectric power output from the prototype window glass. The measured output power for a temperature gradient of 23.5°C is 0.112 μW. The mold to make pellets are shown with the hammer (Inset a). In the prototype, a set of four ball milled followed by hot pressed $Bi_{1.75}Te_{3.25}$ and Sb_2Te_3 alloyed with sulfur nano-materials have been used as thermocouples (Inset b). Copper interconnect has been used for contacting the thermocouples.

in the case of $Bi_{1.75}Te_{3.25}$ samples having angular boundaries and embedded particles.

Electrical resistivity of as-purchased, ball milled and sulfur added samples of $Bi_{1.75}Te_{3.25}$ indicates that the ball milling induces donor like carriers in the powdered samples[11]. It is interesting to note that resistivity is higher for sulfur added sample as compared to the ball milled sample. We believe the difference in the particle size induced by sulfur addition resulted in slightly higher porosity during hot pressing causing an increase in the resistivity. The higher resistivity for sulfur added sample can also be attributed to suppressed carrier concentration with sulfur addition. Electrical resistivity of as-purchased, ball milled and sulfur added samples of Sb_2Te_3 shows a similar trend as that of the $Bi_{1.75}Te_{3.25}$ (Fig. 4b). Since these two samples have comparable particle sizes, the resistivity is similar initially but increases for the ball milled sample as the temperature increases in spite of having higher carrier concentration. The higher electrical resistivity for the ball milled sample is believed to be due to excess micro-structural refinement occurred during ball milling[12], while potential barrier scattering at the grain boundaries may have been responsible for higher electrical conductivity in sulfur added samples in spite of having lower carrier concentration[13].

Seebeck coefficient of as-purchased, ball milled and sulfur added samples of $Bi_{1.75}Te_{3.25}$ shows that the sulfur added sample having lower electrical conductivity due to slight difference in carrier concentration compared to the ball milled counterpart shows relatively higher Seebeck coefficient (Fig. 4c). On the other hand, Seebeck coefficient of as-purchased , ball milled and sulfur added samples of Sb_2Te_3 shows the Seebeck coefficient for the as-purchased and ball milled samples is quite similar whereas it is highest for the sulfur added samples (Fig. 4d). The low carrier concentration for the sulfur added sample has been responsible for the highest Seebeck coefficient. We also expect that potential barrier scattering effect at the grain boundaries may have played a role in deciding the Seebeck coefficient of Sb_2Te_3 samples in addition to the carrier concentrations[13]. The potential barriers have the tendency of filtering the low energy carriers responsible for decreasing Seebeck coefficient. Elimination of these carriers resulted in an overall increase in the Seebeck coefficient of the sulfur added Sb_2Te_3 samples.

Thermal conductivity of as-purchased, ball milled and sulfur added samples of $Bi_{1.75}Te_{3.25}$ shows (as expected) the as-purchased powders with largest particle size has the highest thermal conductivity which reaches as high as 2.75 W/mK around 50 K, but interestingly as the sample reaches room temperature the thermal conductivity decreases down to a very low value similar to the sample with sulfur added to it (Fig. 4e). With the large particle sizes of as-purchased powders, the hot pressing may not have achieved secure packing of particles which may have the tendency to loosen once the sample temperature increases widening the pores inside the sample. It is understandable that the ball milled and sulfur added $Bi_{1.75}Te_{3.25}$ samples have the lower thermal conductivities with the ball milled sample exhibiting values as low as 0.65 W/mK. These low values can be attributed to enhanced phonon scattering at the grain boundaries due to nano-scale size of particles achieved with ball milling. Thermal conductivity of as-purchased, ball milled and sulfur added samples of Sb_2Te_3 shows that nano-structuring brings a two folds decrease in the thermal conductivity of ball milled sample at 50 K, while thermal conductivity of the sulfur added sample is reduced by a factor of 3 (Fig. 4f). For higher temperatures this difference is less pronounced, but the nano-structured samples still have a considerably low value of thermal conductivity due to nano-sized particles and addition of sulfur, that may induce further defect sites causing a deflection and scattering of phonons across a wide range of energies.

Although Seebeck coefficient for ball milled $Bi_{1.75}Te_{3.25}$ nano-material is lower, the *ZT* for ball milled nano-material sample is higher than the sulfur added counterpart, due to higher power factor compared to the sulfur added sample (Fig. 4g). Moreover the ball milled sample has thermal conductivity which is 60% of the sulfur added sample, further enhancing the *ZT* of the ball milled sample. Thermoelectric figure of merit *ZT* for sulfur added Sb_2Te_3 ball milled nano-material samples is the highest for having the highest power factor among all the samples, while the thermal conductivity of the sulfur added samples is also the lowest, all contributing to the increase in its *ZT* (Fig. 4h). For manufacturability purpose, we used moderate energy intensity. However, by more energy intensive process, the *ZT* factor can be significantly increased[14].

The difference between the theoretical and experimental results of the output power is due to the high contact resistance between the thermoelectric pellets and the copper interconnects which is of orders of magnitude higher than the cumulative resistance of all the thermoelectric pellets. Moreover the thermal resistance encountered in interconnects and the silver paste results in significant thermal loss. The hot side of the experimental setup is actually at a temperature lower than indicated by the thermocouple. Therefore the actual temperature gradient is also lower than what is recorded by the thermocouples. We expect that the output power will be increased by three orders of magnitude by reducing the system resistance. The system resistance can be considerably lowered by making interconnects between alternate thermoelectric pellets using deposition techniques such as sputtering or evaporation. It is to be noted we ran the experiments continuously for hours and with day breaks and observe the stable power generation.

Our demonstration shows the successful functionality of a power generating interface which can use the temperature gradient between hot outdoor and relatively cold indoor of a building for generation of useful electric power. As an example, without compromising the original durability of a window glass, a 0.09 m^2 panel can accommodate 2304 holes of 5 mm diameter with reasonable clearance between adjacent holes. Expanding the concept to a larger coverage area for a 5 mm thick glass, with Seebeck coefficient of 200 μV/K and -185 μV/K considered for best p and n type thermoelectric materials, the power output is 304 watts for a 9 m^2 glass window. During the times when cooling systems are switched off, for a 100 m^3 room provided with a 9 m^2 thermoelectric window, it will take 18 minutes to 86 minutes, depending upon the heat transfer coefficient value of air in the range of 25 W/m^2K to 5 W/m^2K respectively, to raise its temperature from 20 Celsius to outside temperature value of 45

Table 1 | Comparison of thermal conductivities of various glasses and thermoelectric materials including the nano-materials used in this work

Material	Reference	Thermal Conductivity (W/mK)
Single Pane Window Glass	[15]	1.1
Corning 7740 Glass	[16]	1.1
Best known n type material	[10]	1.23
Best known p type material	[4]	1.1
Sb_2Te_3 + Sulfur	This work	0.83
$Bi_{1.75}Te_{3.25}$ Ball Milled	This work	0.64

Celsius. The power generated during this duration, using an entirely natural temperature gradient, can be intelligently utilized either for powering up lighter loads or can be stored for later usage. Moreover, with the proposed system mainly intended for extremely hot climates, we expect from our experience of common lifestyle in these regions, the rooms are continuously kept at moderate temperatures keeping cooling systems like air conditioners switched on, at least for the times inhabitants are present in the building.

It might be questioned about the transparency of the window glasses. Typically it is needed to reduce the heat intake through window glasses (by making it tinted) in high temperature areas. Additionally in many citadels and Victorian architectures usage of colored non-transparent glasses are pretty common. So, intelligent design of the embedded thermoelectric system can in fact provide added aesthetic component in window glasses. Finally, in general bismuth telluride and antimony telluride based thermoelectric materials have the same thermal conductivity as the regular window glasses. So, integration of such system will not increase the regular heat intake (Table 1).

In summary, we have demonstrated thermoelectricity generation from window glasses utilizing the temperature difference between the solar heated outdoor and relatively cold indoor of a building. To do so, we have integrated nano-manufactured thermoelectric pellets through drilled holes inside the glass. These pellets are hot pressed from ball milled nano-materials of $Bi_{1.75}Te_{3.25}$ and Sb_2Te_3. We have also explored the possibility of modulating the thermoelectric properties of the nano-powders by addition of 0.6% sulfur to each of the powder matrix in order to improve the thermoelectric performance of our power generating windows. The ball milled samples without the addition of sulfur show the highest figure of merit for $Bi_{1.75}Te_{3.25}$, whereas sulfur addition renders highest figure of merit to Sb_2Te_3. Reducing the system resistance by using deposition techniques like sputtering for interconnecting the thermoelectric legs, orders of magnitude increase in power density can be achieved. Our work on thermoelectric windows provides a complimentary source of electric power to main stream power grid sources capable of running even during sun shine hours or in absence of air-conditioner as long as acceptable temperature difference exists between the outside and inside environment of the building.

Methods

Nano-materials synthesis. In order to prepare nano-materials, commercial available micro-sized powders of each alloy (Sb_2Te_3, $Bi_{1.75}Te_{3.25}$) were purchased from Beijing Cerametek Materials. Four different sets of nano-materials were prepared, two sets by loading Sb_2Te_3 and $Bi_{1.75}Te_{3.25}$ in separate planetary ball mill jars with ball to powder ratio of 15:1 and were subjected to 24 hours of ball milling at a speed of 300 rpm. Remaining two sets of nano-materials of each alloy were prepared by adding 0.6% sulfur by weight to each of the as-purchased alloy powders and were subjected to similar ball mill conditions as the previous two sets.

Hot pressing pellets. Custom made stainless steel molds were fabricated with 5 mm comparable inner diameter to the exact diameter of the holes drilled in glass windows. The maximum height of the molds was 30 mm. Each mold was provided with a corresponding pressing hammer or a rod such that initially the rods may stay at least 3 cm out of the cylinder initially and then goes inward once powder starts to press (Fig. 5 inset). The mold rests on a stainless steel base plate.

Physical characterization of thermoelectric nano-materials and pressed pellets. Compositions of the as-purchased and sulfur mixed samples were analyzed using inductively coupled plasma – optical emission spectroscopy (ICP-OES) (Varian 720 - ES), particle size of as prepared, ball milled and sulfur mixed powders were measured with x– ray diffraction (XRD) (Bruker D8 Advance), structural characterization of powdered samples were carried out using scanning electron microscope (SEM) (FEI Quanta 600), and transmission electron microscope (TEM) (FEI Titan) was used for structural characterization of the pressed pellet samples.

Thermoelectric pellet fabrication. Vertical pellets 5 mm to 7 mm long with diameters of 5 mm were retrieved for each type of powders. All six samples were prepared by pressing at 320°C at 100 MPa for 1 hour using Carver bench top heated press. Additional pellets were pressed to serve as the thermoelectric elements in the subset device for large scale thermoelectric window. In addition to ease of characterization, pressing and retrieving longitudinal pellets facilitate seamless insertion of these thermoelectric elements into holes, with diameters comparable to that of the pellets, drilled in glass or plastic end product.

Thermoelectric window prototype fabrication. A window glass of thickness 5 mm was prepared with a row of 4 drilled holes with diameter of 5 mm and center spacing distance of 9 mm. These holes were filled alternately with hot pressed pellets of Sb_2Te_3 plus sulfur alloy and $Bi_{1.75}Te_{3.25}$ constituting the complimentary n and p type legs of a thermoelectric generator. The length of the pellets was first grounded to 5 mm using a rotary tool fitted with sand paper discs in order to make the length of the pellets precisely equal to the thickness of the glass. The diameter of the pellets was 5 mm which fitted exactly through the holes. The n and p type pellets were connected in series with custom built dog bone shaped copper interconnects using silver paste.

Electrical characterization. To measure power generation, the proto-type device was placed between a glass slide and a heat sink and then placed on a hot plate. Thermal paste was applied between each interface as an attempt to ensure all pellets were subjected to uniform heat flux. Electrical testing of the slide was carried out for various temperature gradients. The hot plate temperature was ramped up in fine intervals with ample thermal delay to allow the opposite surface of the glass slide to attain a stable hot side temperature. The hot side temperature, T_h, and cold side temperature, T_c, were measured using thermocouples placed on each side of the device.

Thermoelectric characterization. The thermoelectric properties of powder samples were also characterized independently before integration into the subset Plexiglas slide. The Quantum Design™ Physical Properties Measurement System (PPMS) was used for these measurements. Pellets of 5 mm long were mounted on the sample puck (Figure 3) for thermal transport measurements. Two - probe technique was used to obtain the Seebeck coefficient and thermal conductivity of the samples. Heater, T1, T2 and cold foot were contacted to a pair of gold coated copper discs, which were attached to the top and bottom faces of the pellets using a two part epoxy which was cured on a hot plate at 150°C for 5 minutes. Electrical conductivity of the pressed pellets was measured using four probe AC resistivity option in PPMS by soldering copper wires to the top face of the pellets.

1. Hudaka, N. S. & Amatucci, G. G. Small-scale energy harvesting through thermoelectric, vibration, and radiofrequency power conversion. *J. Appl. Phys.* **103**, 101301–101324 (1993).
2. Venkatasubramanian, R., Siivola, E., Colpitts, T. & O'Quinn, B. Thin-film thermoelectric devices with high room-temperature figures of merit. *Nature.* **413**, 597–602 (2001).
3. Harman, T. C., Taylor, P. J., Walsh, M. P. & LaForge, B. E. Quantum Dot Superlattice Thermoelectric Materials and Devices. *Science.* **297**, 2229–2232 (2002).
4. Poudel, B., Hao, Q., Ma, Y., Lan, Y. C., Minnich, A., Yu, B., Yan, X., Wang, D. Z., Muto, A., Vashaee, D., Chen, X. Y., Liu, J. M., Dresselhaus, M. S., Chen, G. & Ren, Z. High-thermoelectric performance of nanostructured bismuth antimony telluride bulk alloys. *Science.* **320**, 634–638 (2008).
5. Rowe, D. M., Morgan, D. V. & Kiely, J. H. Miniature low-power/ high-voltage thermoelectric generator. *Electron. Lett.* **25**, 166–168 (1989).

6. Glosch, H., Ashauer, M., Pfeiffer, U. & Lang, W. A thermoelectric converter for energy supply. *Sens. Actuators A.* **74**, 246–250 (1999).
7. Snyder, G. J., Lim, J. R., Huang, C. K. & Fleurial, J. P. Thermoelectric microdevice fabricated by a MEMS-like electrochemical process. *Nat. Mater.* **2**, 528–531 (2003).
8. Bottner, H., Nurnus, J., Gavrikov, A., Kuhner, G., Jagle, M., Kunzel, C., Eberhard, D., Plescher, G., Schubert, A. & Schlereth, K. H. New thermoelectric components using microsystem technologies. *J. Microelectromech. Sys.* **13**, 414–420 (2004).
9. Kishi, M., Nemoto, H., Hamao, T., Yamamoto, M., Sudou, S., Mandai, M. & Yamamoto, S. Micro thermoelectric modules and their application to wristwatches as an energy source. *18th Proc. Int. Conf. Thermoelect.* 301–303 (1999).
10. Mehta, R., Zhang, Y., Karthik, C., Singh, B., Siegel, R. W., Borca-Tasciuc, T. & Ramanath, G. A new class of doped nanobulk high-figure-of-merit thermoelectrics by scalable bottom-up assembly. *Nat. Mater.* **11**, 233–240 (2012).
11. Kuo, C., Hwang, C., Jeng, M., Su, W., Chou, Y. & Ku, J. Thermoelectric transport properties of bismuth telluride bulk materials fabricated by ball milling and spark plasma sintering. *J. Alloy. Compd.* **496**, 687–690 (2010).
12. Ge, Z., Zhang, B., Shang, P., Yu, Y., Chen, C. & Li, J. Enhancing thermoelectric properties of polycrystalline Bi_2S_3 by optimizing a ball-milling process. *J. Electron. Mater.* **40** (5), 1087–1094 (2011).
13. Kishimoto, K., Yamamoto, K. & Koyanagi, T. Influences of potential barrier scattering on the thermoelectric properties of sintered n-type PbTe with a small grain size. *Jpn. J. Appl. Phys.* **42**, 501–508 (2003).
14. Keawprak, N., Suna, Z. M., Hashimoto, H. & Barsoum, M. W. Effect of sintering temperature on the thermoelectric properties of pulse discharge sintered $(Bi_{0.24}Sb_{0.76})_2Te_3$ alloy. *J. Alloy. Compd.* **397**, 236–244 (2005).
15. http://www.saylor.org/site/wp-content/uploads/2011/04/Thermal_conductivity.pdf (Last accessed: September 16, 2012).
16. http://www.nist.gov/data/nsrds/NSRDS-NBS-8.pdf (Last accessed: September 16, 2012).

Acknowledgements

The authors acknowledge financial support under Baseline Research Funding from King Abdullah University of Science and Technology, and the GRP Collaborative Fellow Award (to SI) (GRP-CF-2011-01-S).

Author contributions

MH conceived, designed and directed the research. SI carried out the experiment. SI and KR performed physical characterization of the materials. SI measured the transport property and characterized the system. MH and SI co-wrote the paper. Others reviewed the paper. Everyone participated in the finalized version production.

Additional information

Competing financial interests: The authors declare no competing financial interests.

License: This work is licensed under a Creative Commons Attribution-Non Commercial No Derivative 3.0 Unported License. To view a copy of this license, visit http://creativecommons.org/licenses/by-nc-nd/3.0/

How to cite this article: Inayat, S.B., Rader, K.R. & Hussain, M.M. Nano-materials Enabled Thermoelectricity from Window Glasses. *Sci. Rep.* **2**, 841; DOI:10.1038/srep00841 (2012).